



HCOOH decomposition over the pure and Ag-modified Pd nanoclusters: Insight into the effects of cluster size and composition on the activity and selectivity

Min Yang^a, Baojun Wang^a, Maohong Fan^{b,c,d}, Riguang Zhang^{a,*}

^a Key Laboratory of Coal Science and Technology of Ministry of Education and Shanxi Province, Taiyuan University of Technology, Taiyuan 030024, Shanxi, PR China

^b Departments of Chemical and Petroleum Engineering, University of Wyoming, Laramie, WY 82071, USA

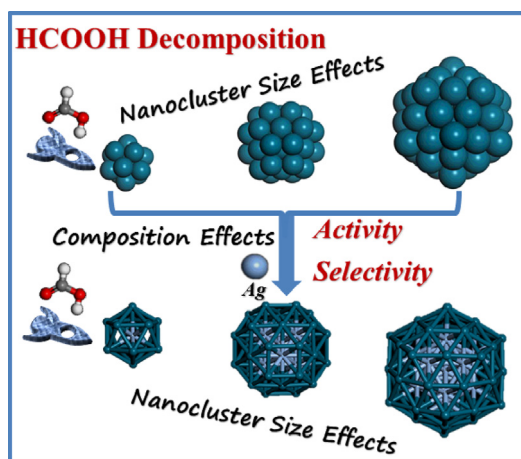
^c School of Civil and Environmental Engineering, Georgia Institute of Technology, Atlanta, GA 30332, USA

^d School of Energy Resources, University of Wyoming, Laramie, WY 82071, USA

HIGHLIGHTS

- The effects of cluster size and composition on the performance of HCOOH decomposition were examined.
- CO₂ formation is favored in kinetics than CO formation on the pure and Ag-modified Pd nanoclusters.
- The small size of the pure and Ag-modified Pd nanoclusters exhibit higher activity and selectivity toward CO₂ formation.
- The Ag composition improves the activity and selectivity toward CO₂ formation.
- The better activity and selectivity is attributed to that the *d*-band center is more close to Fermi level.

GRAPHICAL ABSTRACT



ARTICLE INFO

Article history:

Received 16 March 2020
 Received in revised form 8 July 2020
 Accepted 1 August 2020
 Available online 5 August 2020

Keywords:

HCOOH decomposition
 Catalytic performance
 Pd-based nanocluster
 Nanocluster size
 Composition

ABSTRACT

This work is designed to examine the size and composition effects of the pure and Ag-modified Pd nanoclusters on the activity and selectivity of HCOOH decomposition using DFT calculations and microkinetic modeling. Pd_n (n = 13,38,55) and Ag_m@Pd_n (m + n = 13,38,55) nanoclusters are considered. The results show that HCOOH decomposition dominantly undergoes COOH intermediate instead of HCOO intermediate, and CO₂ formation is more favorable than CO formation. The pure and Ag-modified Pd nanoclusters with the small size exhibit higher activity and selectivity toward CO₂ formation; meanwhile, when the nanocluster size is the same, compare to the pure Pd, the Ag composition improves the activity and selectivity toward CO₂ formation, and decreases the usage of noble-metal Pd. The better catalytic performance is attributed to that the *d*-band center is more close to the Fermi level. The results provide a method for improving catalytic performance of Pd-based nanoclusters by adjusting the size and core composition of the nanocluster.

© 2020 Elsevier Ltd. All rights reserved.

* Corresponding author.

E-mail address: zhangriguang@tyut.edu.cn (R. Zhang).

1. Introduction

Formic acid (HCOOH) fuel cells are widely studied as green energy (Fellay et al., 2008; Zhang et al., 2010; Ha et al., 2005; Uhm et al., 2008), in which Pd-based catalysts exhibit better activity and selectivity toward HCOOH decomposition (Mori et al., 2013; Yang et al., 2019; Hu et al., 2019; Choi et al., 2019; Rice et al., 2002), HCOOH decomposition mainly goes through direct dehydrogenation pathway ($\text{HCOOH} \rightarrow \text{CO}_2 + \text{H}_2$) to produce CO_2 and H_2 (Wang et al., 2014; Brandt et al., 2008). Whereas the pure Pd catalyst is unstable when HCOOH is operated at high concentration due to the rapid and gradual dissolution of Pd in oxidation state and slow intermediate adsorption under acid conditions (Wang et al., 2011; El-Nagar et al., 2016; Yu and Pickup, 2009). Nowadays, Pd-based bimetallic catalysts, such as Ni-Pd (Gao et al., 2011; Shen et al., 2013), Au-Pd (Yu et al., 2014; Gu et al., 2011), Ag-Pd (Lu and Chen, 2012; Tedsree et al., 2011), Sn-Pd (Wang et al., 2016; Sun et al., 2015) and Cu-Pd (Dai and Zou, 2011; Wu et al., 2016), have attracted much attention for HCOOH decomposition, which improved the catalyst stability, catalytic performance, and decreased the usage of noble-metal Pd due to the synergistic interaction between two metals (Huang et al., 2010; Feng et al., 2016; Maroun et al., 2001; Fan et al., 2016; Liu et al., 2017). Among them, the Ag-Pd bimetallic catalysts prepared by Lu et al. (Lu and Chen, 2012) exhibited strong catalytic activity and high current density for HCOOH oxidation, as well as the strong resistance to CO poisoning.

On the other hand, the core-shell nanocluster catalysts with unique structures have become one of the most promising catalysts. Li et al. (Li et al., 2014) concluded that the core-shell Cu@Pd catalysts presented higher activity by four times than the pure Pd catalyst toward HCOOH decomposition. Zhou et al. (Zhou et al., 2008) found that the core-shell PdAu/C catalysts are favorable for HCOOH decomposition to produce H_2 and inhibit CO poisoning. Huang et al. (Huang et al., 2018) showed that the core-shell PdAg@Pd nanotubes exhibited better catalytic performance toward HCOOH decomposition compared to PdAg nanotubes, which is attributed to the unique surface and electronic structure. Tedsree et al. (Tedsree et al., 2011) synthesize a series of M@Pd (M = Ru, Rh, Ag, Au, Pt) catalysts, in which the Ag@Pd catalyst showed weak CO poisoning ability. Recently, our studies (Yang et al., 2020) have investigated HCOOH decomposition over a series of core-shell bimetallic M@Pd (M = Cu, Au, Co, Ni, Ag and Al) catalysts by DFT calculations and microkinetic modeling, among them, Ag@Pd has the highest activity and selectivity of CO_2 formation and shows a strong anti-CO poisoning ability. On the other hand, the particle size of core-shell nanocluster has an important influence on the stability and catalytic properties, such as Zhao et al. (Zhao et al., 2017) studied the size effect of Cu catalyst including the Cu_{13} , Cu_{38} , Cu_{55} nanoclusters and Cu(111) surface on C_2H_2 selective hydrogenation.

Further, for the pure and Ag-modified Pd nanoclusters, Huang et al. (Huang et al., 2009) showed that the activity of the size-controlled Pd/C catalysts for HCOOH decomposition depends on the catalyst particle size, however, to our knowledge, only the Pd_7 (Li et al., 2012) and Pd_{55} (Liu et al., 2017) nanoclusters are reported; meanwhile, HCOOH decomposition via the COOH intermediate has not been mentioned. Thus, up to now, the fundamental understanding about the particle size effects of the pure and Ag-modified Pd catalysts on the catalytic activity and selectivity of HCOOH decomposition are still unclear due to the lack of incomplete information over different sizes of the pure and Ag-modified Pd nanoclusters.

This work is designed to solve above issues by investigating the selectivity and activity of HCOOH decomposition over different

sizes of the pure and Ag-modified Pd nanoclusters, which include the Pd_n ($n = 13, 38, 55$) and $\text{Ag}_m\text{@Pd}_n$ ($m + n = 13, 38, 55$) nanoclusters; here the density functional theory calculations and microkinetic modeling were employed. It is expected that the results can provide a clue for the rational design of high-performance core-shell Pd-based nanoclusters by controlling their sizes and compositions.

2. Computational details

2.1. Computational method

The VASP 5.2.2 is used for the periodic theoretical calculation (Kresse and Furthmüller, 1996a, 1996b). In the whole calculation process, the pseudopotential uses projector augmented wave (PAW), the generalized gradient approximation with the Perdew-Burke-Ernzerhof (GGA-PBE) is used to describe the exchange and correlation (Blöchl, 1994; Perdew and Wang, 1992; Perdew et al., 1996). The plane wave cutoff energy is set to 400 eV and the Brillouin zone was sampled with a $1 \times 1 \times 1$ k -point grid for the total energies. For the geometry optimization, the convergence results were obtained when the total energy change between two continuous steps is less than 1×10^{-5} eV and the force constant is less than 0.03 eV Å. The climbing-image nudged elastic band (CI-NEB) (Sheppard et al., 2012, 2008) and dimer methods (Henkelman and Jónsson, 1999; Olsen et al., 2004) were used to search for transition state (TS), which corresponds to only one imaginary frequency. The details for calculating relevant energy at 298 K are presented in the Supplementary Material.

2.2. Surface model

For the pure Pd nanoclusters, experimental studies showed that the Pd_{13} , Pd_{38} and Pd_{55} clusters are the stable magic number nanoclusters (Soler et al., 2000; Nayak et al., 1997), which not only model different sizes of the nanocluster, but also present different surface structures. In this study, the Pd_{13} , Pd_{38} and Pd_{55} nanoclusters with the corresponding diameters of about 5, 8 and 10 Å were used to investigate the size effect of Pd nanocluster on the catalytic performance of HCOOH decomposition. Meanwhile, aiming at considering the effect of the composition in the core-shell M@Pd catalysts, different sizes of core-shell $\text{Ag}_1\text{@Pd}_{12}$, $\text{Ag}_6\text{@Pd}_{32}$ and $\text{Ag}_{13}\text{@Pd}_{42}$ catalysts were constructed using Ag atoms replacing Pd atoms in the central groups of Pd_{13} , Pd_{38} and Pd_{55} nanoclusters. The most stable configurations of these nanoclusters and the corresponding adsorption sites were presented in Fig. 1.

Both Pd_{13} and $\text{Ag}_1\text{@Pd}_{12}$ nanoclusters are the icosahedral structures, including twenty (111) faces (Karabacak et al., 2003; Rapps et al., 2013) with 12 atoms in the shell and one atom in the core, all the shell atoms have the same coordination number 6. Both Pd_{38} and $\text{Ag}_6\text{@Pd}_{32}$ nanoclusters with the truncated octahedron structure are more stable than other isomers (Zhu et al., 2015; Kumar and Kawazoe, 2003), the shell consists of 24 Pd atoms at the top of (100) plane and 8 Pd atoms at the center of (111) plane; the coordination number of the shell Pd atom is 6 and 9. For the Pd_{55} and $\text{Ag}_{13}\text{@Pd}_{42}$ nanoclusters, the most stable structure is also a highly symmetrical structure (Zhu et al., 2015; Kumar and Kawazoe, 2003; Zhao et al., 1995), in which the outmost layer has 42 atoms, the second layer has 12 atoms, and the core has an atom; accordingly, the coordination number of the shell Pd atom is 6 and 8.

Further, in order to analyze the effect of nanocluster size on the catalytic performance of HCOOH decomposition, previous studies about HCOOH decomposition over the Pd(111) and Ag@Pd(111) surfaces used to model very large sizes of the pure and Ag-

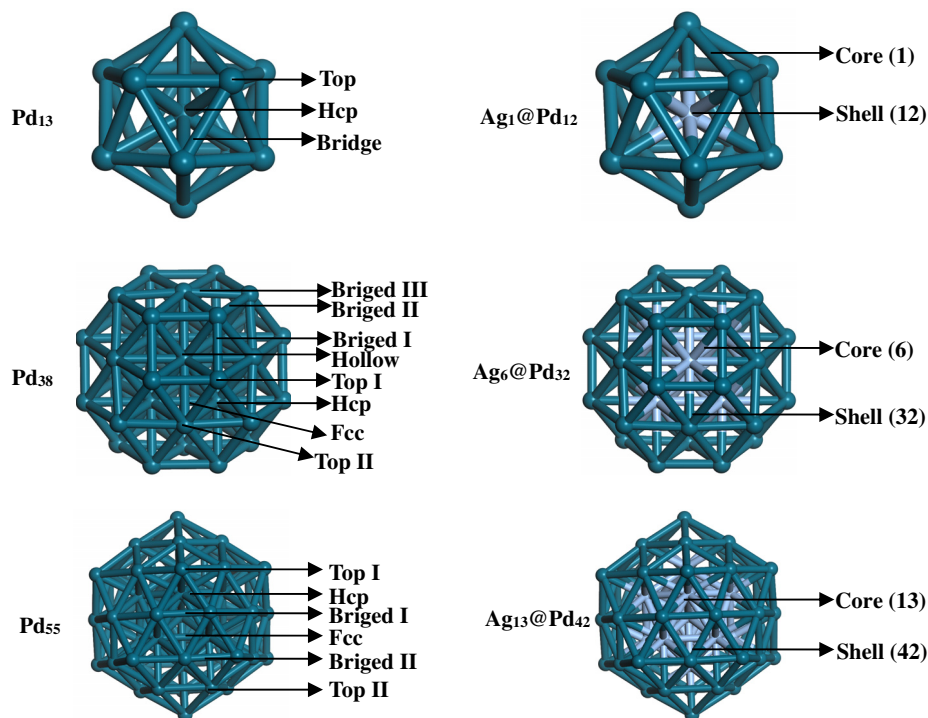


Fig. 1. Optimized structures for different sizes of Pd₁₃, Pd₃₈, Pd₅₅, Ag₁@Pd₁₂, Ag₆@Pd₃₂, Ag₁₃@Pd₄₂ nanoclusters, as well as the adsorption sites. Blue and silvery balls denote Pd and Ag atoms, respectively.

modified Pd nanoclusters (Yang et al., 2020) were also considered and compared, all surface Pd atoms over the Pd(111) and Ag@Pd(111) surfaces correspond to the coordination number of 9.

3. Results and discussion

3.1. The proposed pathway of HCOOH decomposition

The adsorbed HCOOH decomposes into different products via various intermediates based on different decomposition pathways. Since the first step of HCOOH decomposition involves the C-H, O-H and C-OH bond cleavage, three possible pathways for HCOOH decomposition were proposed, as shown in Scheme 1.

Path 1 is the O-H bond scission of HCOOH via the HCOO intermediate; Path 2 is the C-H bond scission via the COOH intermediate; Path 3 is the C-OH bond scission via the HCO intermediate. CO₂ + H₂ formation may go through the HCOO and COOH intermediates; whereas CO + H₂O formation may undergoes the COOH and HCO intermediates. However, previous studies (Yang et al., 2020; Zhang et al., 2012; Singh et al., 2014; Qi et al., 2015) showed

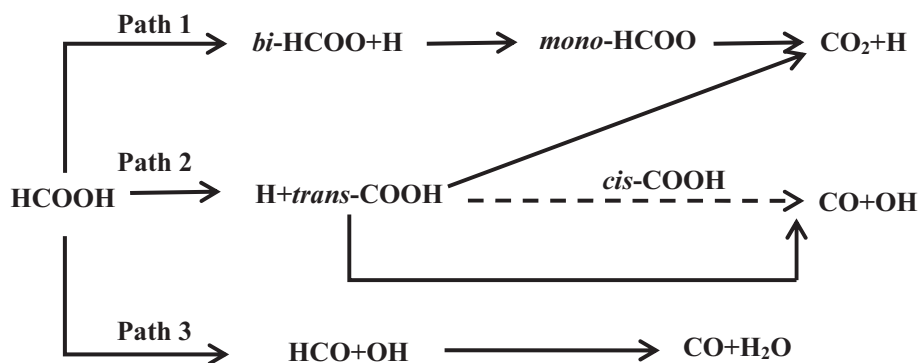
that CO formation via the HCO intermediates on the pure Pd and core-shell M@Pd (M = Cu, Au, Co, Ni, Ag, Al) catalysts is difficult to occur compared to CO formation via the COOH intermediates. Thus, Path 3 via the HCO intermediate is excluded in this study, only HCOOH decomposition via the HCOO and COOH intermediates are considered.

Fig. S1 presents the stable adsorption configurations of possible species, the corresponding adsorption free energies and adsorption sites are listed in Table S1. The activation barrier and reaction energy of elementary reaction in HCOOH decomposition are listed in Table S2.

3.2. HCOOH decomposition over the pure Pd_n (n = 13, 38, 55) nanoclusters

3.2.1. HCOOH decomposition via the HCOO intermediate

As shown in Figs. 2–4, in Path I, HCOOH is firstly decomposed into the co-adsorbed *bi*-HCOO and H species via the transition state TSx-1 (x = 1–3), which have activation barriers of 23.9, 37.4 and



Scheme 1. Proposed reaction mechanism of HCOOH decomposition.

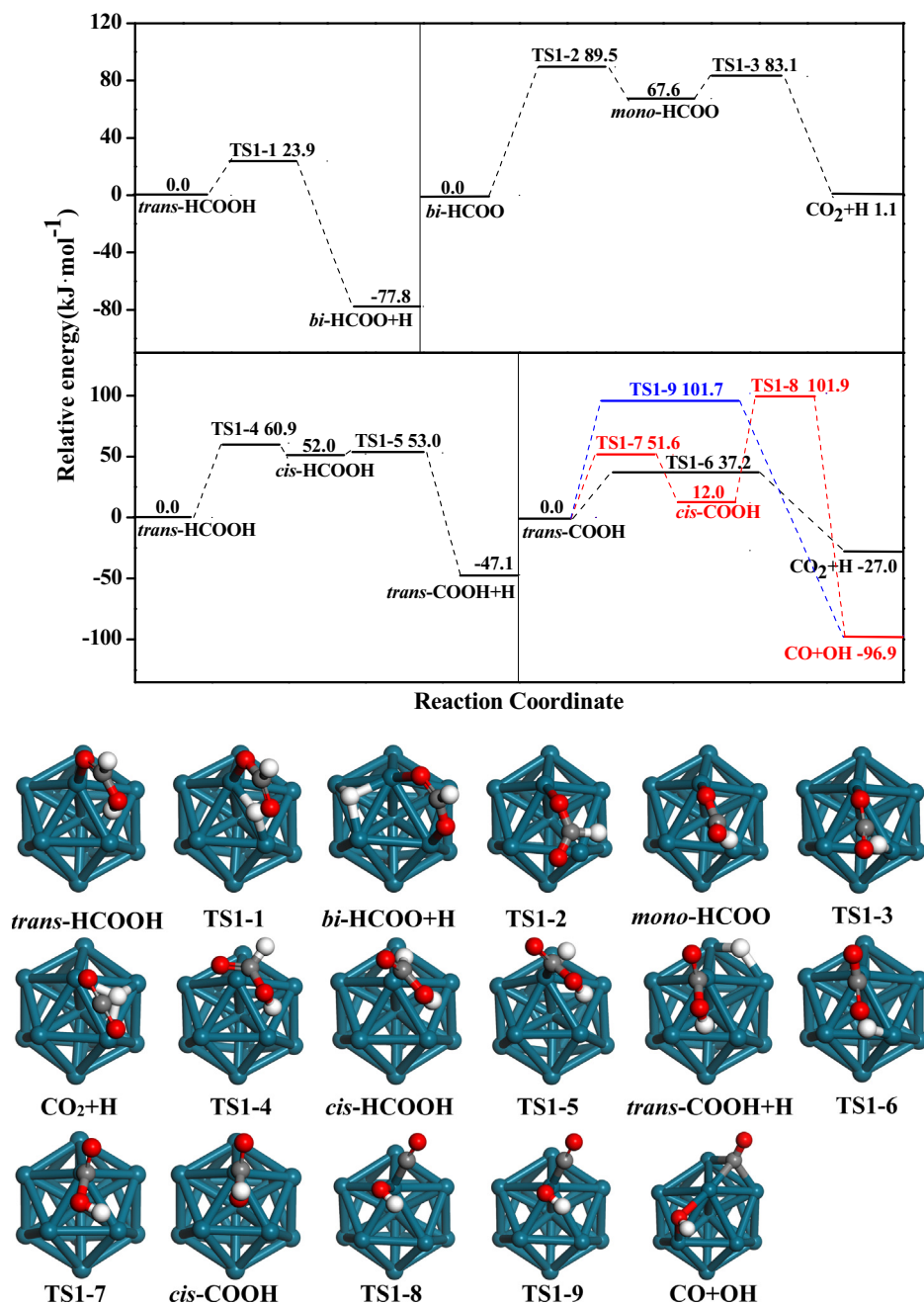


Fig. 2. Potential energy profile of HCOOH decomposition via the HCOO and COOH intermediates with the initial state, transition states and final states on Pd₁₃ nanocluster at 298 K.

41.7 kJ·mol⁻¹ over the Pd₁₃, Pd₃₈ and Pd₅₅, respectively, it is exothermic by 77.8, 35.4 and 39.6 kJ·mol⁻¹, respectively. Meanwhile, previous studies on Pd(111) surface (Yang et al., 2020) showed that this reaction has activation barrier of 50.6 kJ·mol⁻¹ and it is slightly exothermic by 1.2 kJ·mol⁻¹.

Then, beginning with the *bi*-HCOO intermediates, to facilitate the H atom falling onto the nanoclusters, the first step is to form *mono*-HCOO via the TSx-2(x = 1–3) with the close activation barriers of 89.5, 93.8 and 85.1 kJ·mol⁻¹ over the Pd₁₃, Pd₃₈ and Pd₅₅, respectively, which is also close to the activation barrier of 92.8 kJ·mol⁻¹ on Pd(111) surface (Yang et al., 2020). In this step, the conversion of HCOO intermediates by different adsorption configurations agrees with the previous studies (Wang et al., 2014; Zhang et al., 2019; Samjeske and Osawa, 2005; Gao et al.,

2012; Herrero and Feliu, 2018), which were also experimentally observed over other Pd-based and Pt-based catalysts (Vela et al., 1992; Chen et al., 2006; Duan et al., 2016). Further, the target product CO₂ is produced by *mono*-HCOO decomposition via the TSx-3(x = 1–3) corresponding to the close activation barriers of 15.5, 19.3 and 18.4 kJ·mol⁻¹ over the Pd₁₃, Pd₃₈ and Pd₅₅, respectively, this reaction is strongly exothermic by 66.5, 103.5 and 101.7 kJ·mol⁻¹, respectively; the activation barrier on Pd(111) surface is 7.9 kJ·mol⁻¹ (Yang et al., 2020). Thus, *bi*-HCOO dehydrogenation to form CO₂ (HCOO → CO₂ + H) corresponds to the overall activation barriers of 89.5, 96.3, 85.1 and 92.8 kJ·mol⁻¹ with reaction energies of 1.1, -26.5, -39.9 and -71.4 kJ·mol⁻¹ over the Pd₁₃, Pd₃₈, Pd₅₅ and Pd(111) (Yang et al., 2020), respectively.

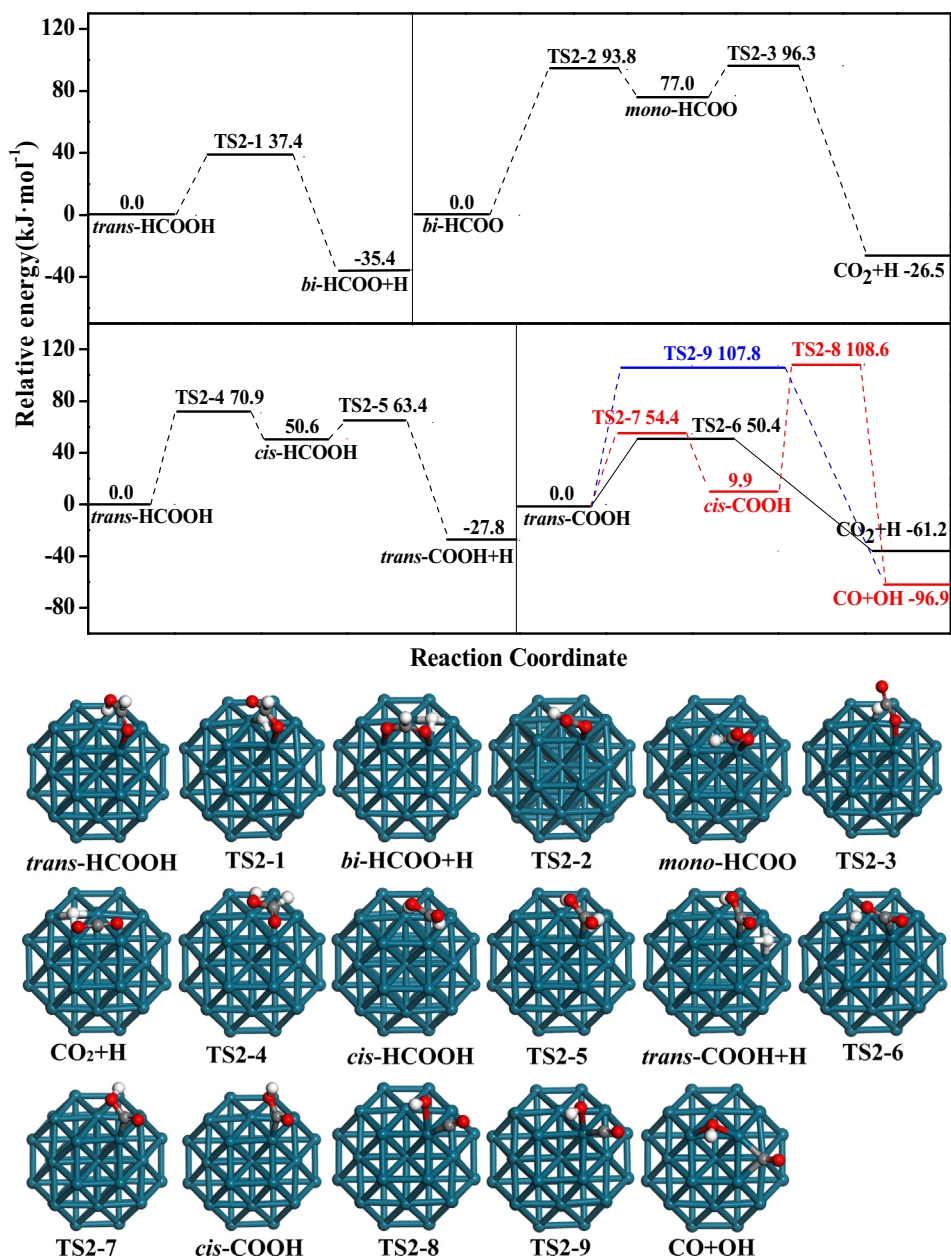


Fig. 3. Potential energy profile of HCOOH decomposition via the HCOO and COOH intermediates with the initial state, transition states and final states on Pd₃₈ nanocluster at 298 K.

Above results show that the reaction of $\text{HCOO} \rightarrow \text{CO}_2 + \text{H}$ is the rate-controlled step for HCOOH decomposition via the HCOO intermediate, meanwhile, the size of Pd nanoclusters affect the activation barrier of $\text{trans-HCOOH} \rightarrow \text{HCOO} + \text{H}$ and $\text{HCOO} \rightarrow \text{CO}_2 + \text{H}$, and therefore alter the catalytic activity of HCOOH decomposition via the HCOO intermediate, especially, the first step of HCOOH decomposition ($\text{trans-HCOOH} \rightarrow \text{bi-HCOO} + \text{H}$), the differences of activation barrier and reaction energy over different sizes of Pd nanoclusters is mainly attributed to the adsorption stability of co-adsorbed HCOO and H species, in which both *bi-HCOO* and H species are adsorbed at the stepped plane over the Pd₁₃, Pd₃₈ and Pd₅₅ nanoclusters, whereas those are adsorbed at the flatted Pd (111) plane.

3.2.2. HCOOH decomposition via the COOH intermediate

In Path II, *trans-HCOOH* is firstly isomerized to form *cis-HCOOH* aiming at facilitating the C-H bond breakage via the TS_{x-4} ($x = 1-3$),

which is also confirmed by previous studies on PtAu catalysts (Duan et al., 2016); this reaction has the activation barriers of 60.9, 70.9, 72.5 and 70.8 $\text{kJ}\cdot\text{mol}^{-1}$ over the Pd₁₃, Pd₃₈, Pd₅₅ nanoclusters and Pd(111) (Yang et al., 2020), respectively.

Then, the C-H bond breakage of *cis-HCOOH* can produce the co-adsorbed *trans-COOH* and H species via the TS_{x-5} ($x = 1-3$), which correspond to the activation barriers of 1.0, 12.8, 16.5 and 31.5 $\text{kJ}\cdot\text{mol}^{-1}$, and it is exothermic by 99.1, 78.4, 66.9 and 57.3 $\text{kJ}\cdot\text{mol}^{-1}$, respectively. Thus, $\text{trans-HCOOH} \rightarrow \text{COOH} + \text{H}$ has the overall activation barriers of 60.9, 70.9, 70.1 and 70.8 $\text{kJ}\cdot\text{mol}^{-1}$ with the reaction energies of -47.1 , -27.8 , -36.1 and -31.6 $\text{kJ}\cdot\text{mol}^{-1}$ over the Pd₁₃, Pd₃₈, Pd₅₅ and Pd(111), respectively. Starting with the *trans-COOH* intermediates, it goes through the O-H or C-OH bond cleavage to produce CO₂ or CO.

For CO₂ formation via the TS_{x-6} ($x = 1-3$), the activation barriers are 37.2, 50.4, 61.0 and 60.1 $\text{kJ}\cdot\text{mol}^{-1}$ over the Pd₁₃, Pd₃₈, Pd₅₅ and Pd(111), respectively, suggesting that the activity of CO₂ formation

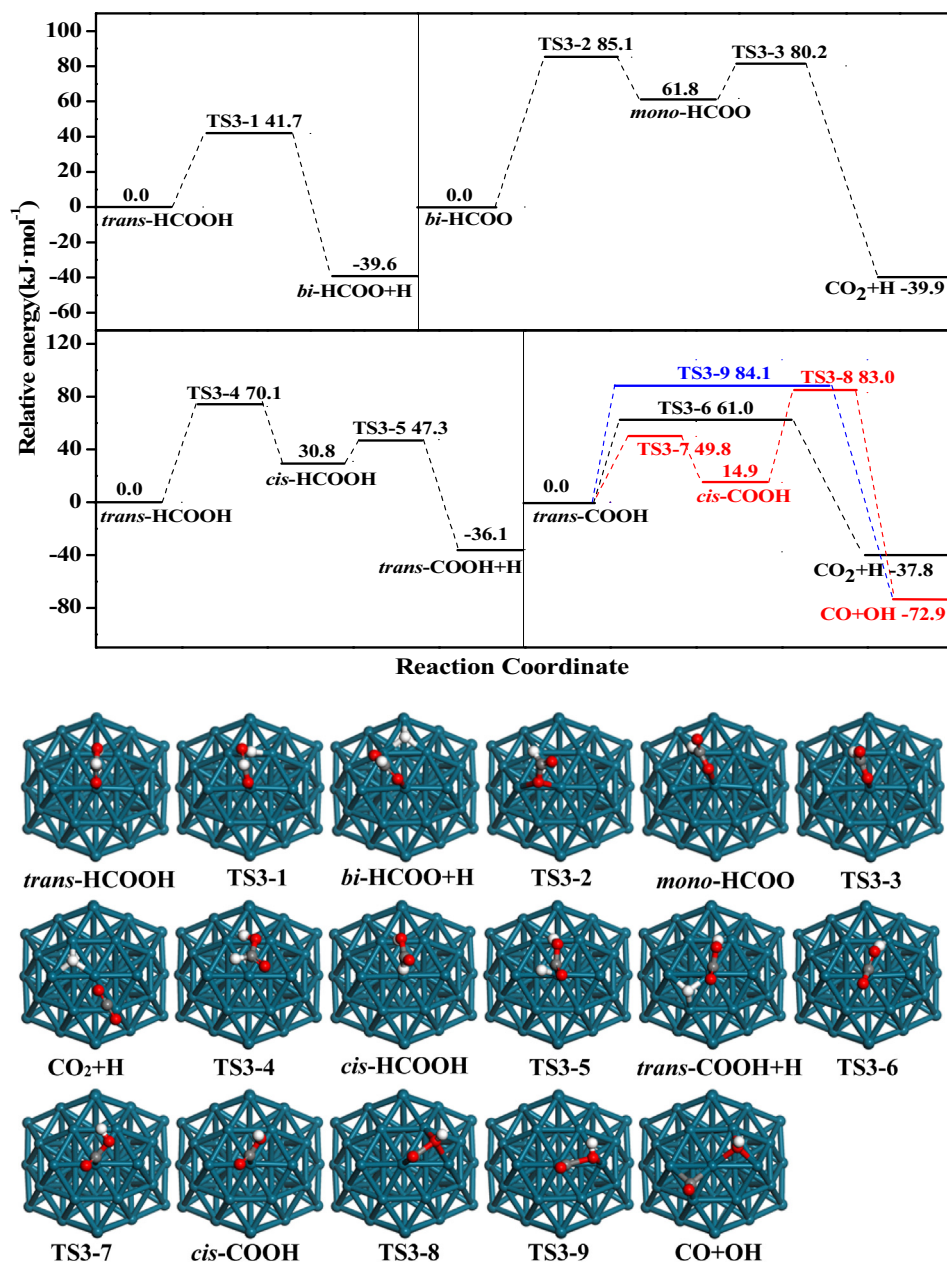


Fig. 4. Potential energy profile of HCOOH decomposition via the HCOO and COOH intermediates with the initial state, transition states and final states on Pd₅₅ nanocluster at 298 K.

decreases with the size increasing of Pd nanoclusters. Meanwhile, $trans\text{-HCOOH} \rightarrow \text{COOH} + \text{H}$ is the rate-controlled step for HCOOH decomposition via the COOH intermediate to form CO₂.

For CO formation, two routes exist, one is the isomerization of $trans\text{-COOH}$ to $cis\text{-COOH}$ (TSx-7(x = 1–3)), followed by the dissociation of $cis\text{-COOH}$ intermediate (TSx-8(x = 1–3)); the other is the dissociation of $trans\text{-COOH}$ via the TSx-9(x = 1–3). For the former, $trans\text{-COOH}$ is firstly isomerized to $cis\text{-COOH}$ by the O-H bond rotation, followed by the O-H bond cleavage of $cis\text{-COOH}$ to form CO, the overall activation barriers are 101.9, 108.6, 83.0 and 81.8 kJ·mol⁻¹, and it is exothermic by 96.9, 96.9, 72.9 and 10.9 kJ·mol⁻¹ over the Pd₁₃, Pd₃₈, Pd₅₅ and Pd(111), respectively. The latter route has the activation barriers of 101.7, 107.8, 84.1 and 79.1 kJ·mol⁻¹ over the Pd₁₃, Pd₃₈, Pd₅₅ and Pd(111), respectively. It is found that two routes of CO formation is energetically competitive; moreover, the structures of TSx-8 and TSx-9 are similar and the C-O bond length of CO is close over the Pd₁₃ (1.934 vs.

1.908 Å), Pd₃₈ (2.022 vs. 2.006 Å), Pd₅₅ (1.812 vs. 1.856 Å) and Pd(111) (2.000 vs. 2.002 Å) (Yang et al., 2020), respectively. Thus, CO formation has two parallel routes, the activity of CO formation increase with the size increasing of Pd nanoclusters. The reaction $trans\text{-COOH} \rightarrow \text{CO} + \text{OH}$ is the rate-controlled step for HCOOH decomposition via the COOH intermediate to form CO.

3.3. HCOOH decomposition over the Ag₁@Pd₁₂, Ag₆@Pd₃₂ and Ag₁₃@Pd₄₂

3.3.1. HCOOH decomposition via the HCOO intermediate

See Figs. 5–7, in Path I, $trans\text{-HCOOH} \rightarrow \text{HCOO} + \text{H}$ via the TSx-1 (x = 4–6) has the activation barriers of 22.3, 44.8 and 32.1 kJ·mol⁻¹, and it is exothermic by 71.1, 46.9 and 44.1 kJ·mol⁻¹ over the Ag₁@Pd₁₂, Ag₆@Pd₃₂ and Ag₁₃@Pd₄₂, respectively. Meanwhile, the acti-

vation barrier is $32.8 \text{ kJ}\cdot\text{mol}^{-1}$ on $\text{Ag@Pd}(111)$ surface (Yang et al., 2020), and it is exothermic by $27.5 \text{ kJ}\cdot\text{mol}^{-1}$.

Then, starting from *bi*-HCOO intermediates, $\text{HCOO} \rightarrow \text{CO}_2 + \text{H}$ has the overall activation barriers of 96.2, 90.6, 82.5 and $61.4 \text{ kJ}\cdot\text{mol}^{-1}$ with the reaction energies of -2.8 , -19.8 , -56.5 and $-95.1 \text{ kJ}\cdot\text{mol}^{-1}$ on the $\text{Ag}_1\text{@Pd}_{12}$, $\text{Ag}_6\text{@Pd}_{32}$, $\text{Ag}_{13}\text{@Pd}_{42}$ and $\text{Ag@Pd}(111)$, respectively. These results show that $\text{HCOO} \rightarrow \text{CO}_2 + \text{H}$ is the rate-controlled step for HCOOH decomposition via the HCOO intermediate, and the activity of CO_2 formation increases with the size increasing of Ag-modified Pd nanoclusters.

3.3.2. HCOOH decomposition via the COOH intermediate

In Path II, the reaction of *trans*-HCOOH \rightarrow *trans*-HCOO + H via the *cis*-HCOOH intermediate has the overall activation barriers of

57.6, 64.8, 59.2 and $67.5 \text{ kJ}\cdot\text{mol}^{-1}$ with reaction energies of -47.1 , -29.0 , -41.7 and $-57.5 \text{ kJ}\cdot\text{mol}^{-1}$ over the $\text{Ag}_1\text{@Pd}_{12}$, $\text{Ag}_6\text{@Pd}_{32}$, $\text{Ag}_{13}\text{@Pd}_{42}$ and $\text{Ag@Pd}(111)$ (Yang et al., 2020), respectively.

Starting with the *trans*-COOH intermediates, CO_2 formation via the TSx-6($x = 4 \sim 6$) corresponds to the activation barriers of 41.7, 50.1, 49.4 and $46.7 \text{ kJ}\cdot\text{mol}^{-1}$ over the $\text{Ag}_1\text{@Pd}_{12}$, $\text{Ag}_6\text{@Pd}_{32}$, $\text{Ag}_{13}\text{@Pd}_{42}$ and $\text{Ag@Pd}(111)$, respectively. Meanwhile, the reaction of *trans*-HCOOH \rightarrow COOH + H is the rate-controlled step for HCOOH decomposition via the COOH intermediate to form CO_2 .

Starting with the *trans*-COOH intermediates, for CO formation, the C-OH bond cleavage of *trans*-COOH to form CO has the activation barriers of 99.2, 117.2, 91.1 and $83.4 \text{ kJ}\cdot\text{mol}^{-1}$ over the $\text{Ag}_1\text{@Pd}_{12}$, $\text{Ag}_6\text{@Pd}_{32}$, $\text{Ag}_{13}\text{@Pd}_{42}$ and $\text{Ag@Pd}(111)$, respectively. Alternatively, the isomerization of *trans*-COOH to *cis*-COOH, fol-

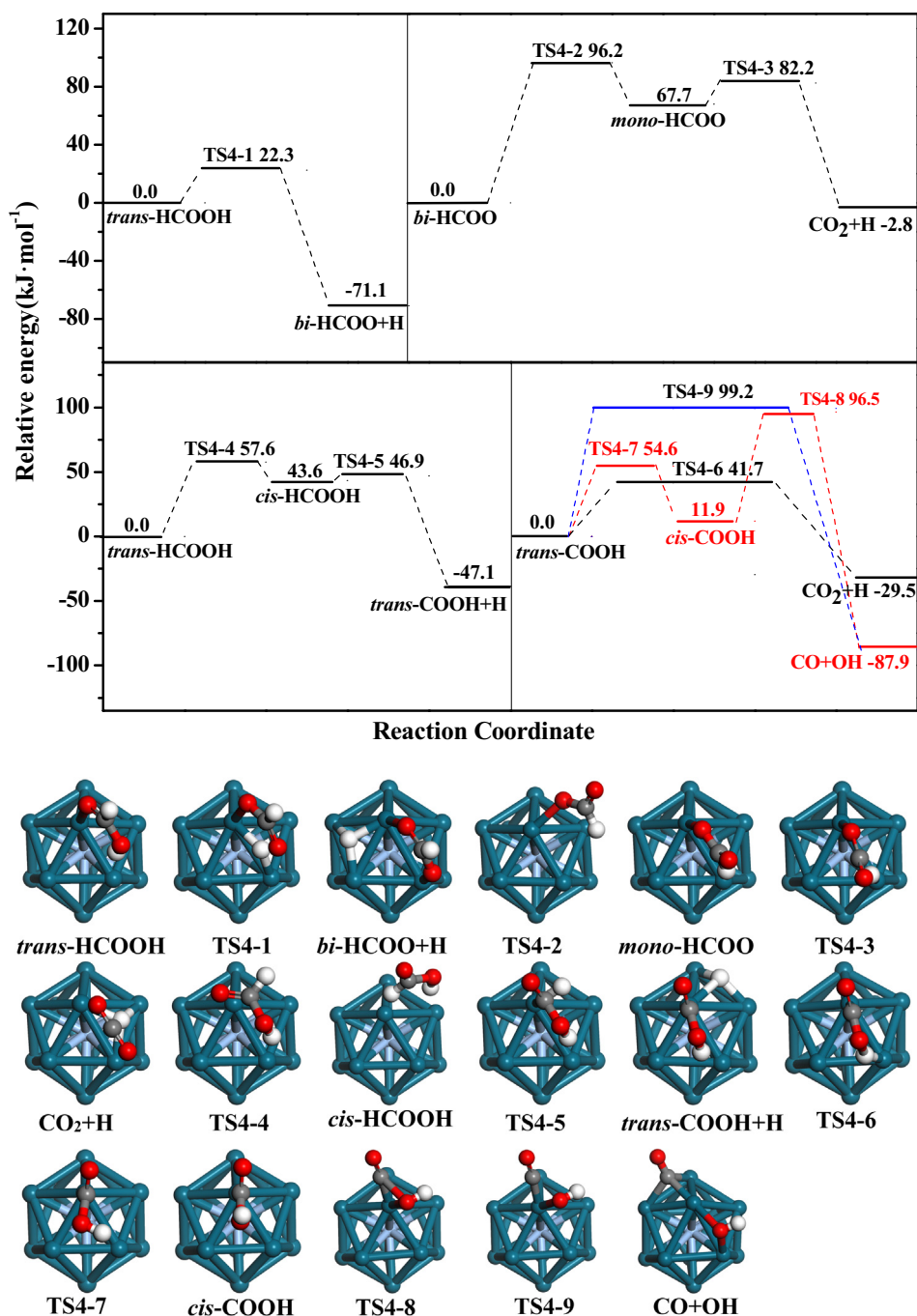


Fig. 5. Potential energy profile of HCOOH decomposition via the HCOO and COOH intermediates with the initial state, transition states and final states on $\text{Ag}_1\text{@Pd}_{12}$ at 298 K.

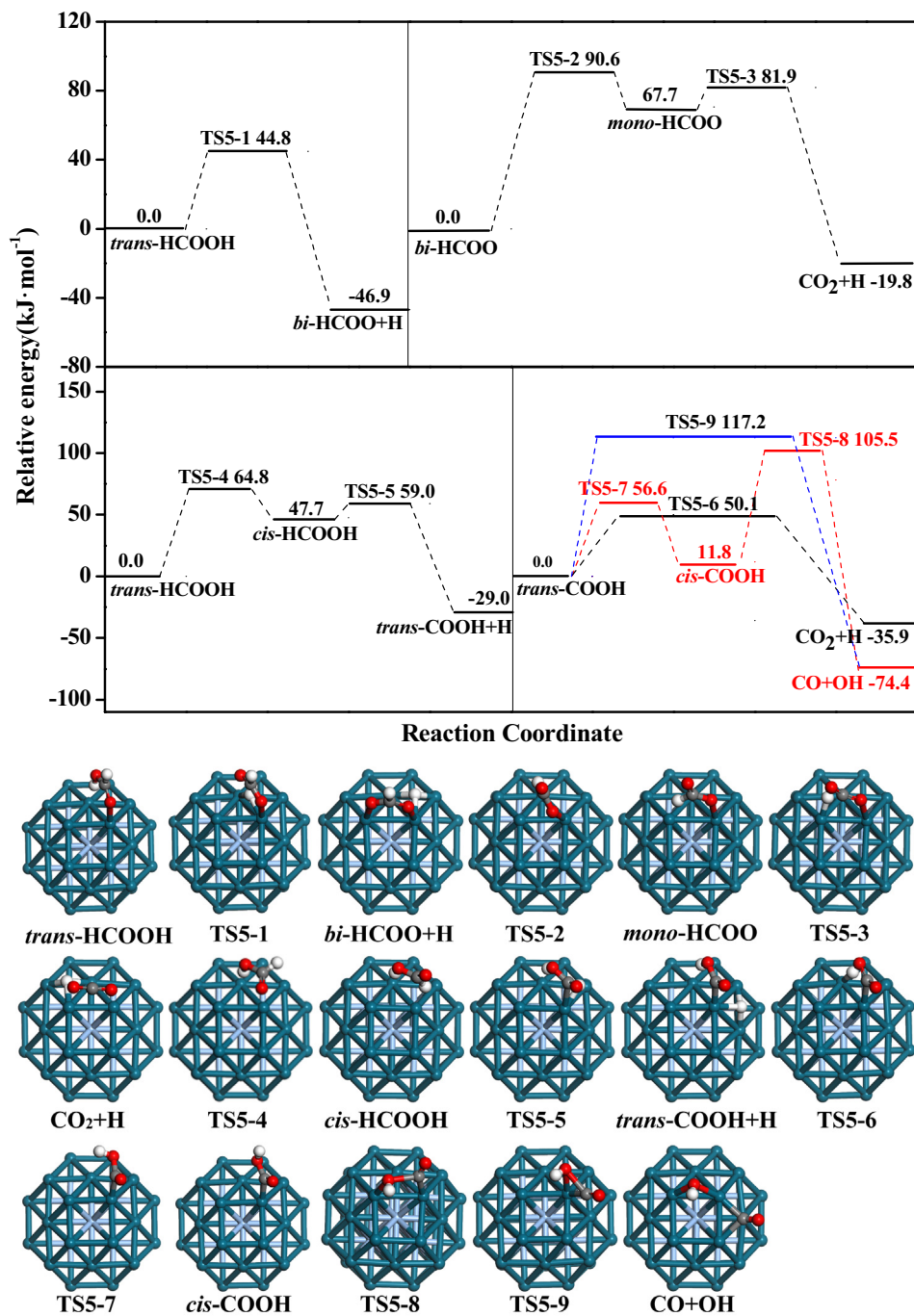


Fig. 6. Potential energy profile of HCOOH decomposition via the HCOO and COOH intermediates with the initial state, transition states and final states on Ag₆@Pd₃₂ at 298 K.

lowed its O-H bond cleavage to form CO, has the overall activation barriers are 96.5, 105.5, 84.0 and 86.7 kJ·mol⁻¹, and it is exothermic by 87.9, 74.4, 95.6 and 44.3 kJ·mol⁻¹ over the Ag₁@Pd₁₂, Ag₆@Pd₃₂, Ag₁₃@Pd₄₂ and Ag@Pd(111), respectively. These results show that the route via the *cis*-COOH intermediate is slightly favorable in kinetics than *trans*-COOH direct dissociation. *trans*-COOH → CO + O-H is the rate-controlled step for HCOOH decomposition via the COOH intermediate to form CO.

3.4. General discussion

3.4.1. The effects of cluster size and composition on the optimal route

For CO formation, as shown in Figs. 2–7, HCOOH decomposition mainly goes through COOH intermediate to produce CO over differ-

ent sizes of Pd and Ag-modified Pd nanoclusters, in which two routes exist, one is *trans*-COOH dissociation; the other is the dissociation of *cis*-COOH intermediate from the isomerization of *trans*-COOH. Over the Pd₁₃, Pd₃₈ and Pd₅₅, these two routes are energetically competitive and simultaneously contribute to CO formation. However, the route via the *cis*-COOH intermediate to form CO is favorable than *trans*-COOH direct dissociation to form CO over the Ag₁@Pd₁₂, Ag₆@Pd₃₂ and Ag₁₃@Pd₄₂ nanoclusters, namely, the route via the *cis*-COOH intermediate dominantly contribute to CO formation. Further, *trans*-COOH → CO + OH is the rate-controlled step for HCOOH decomposition via the COOH intermediate to produce CO.

For CO₂ formation, as shown in Figs. 2–7, based on the rate-controlled step of HCOOH decomposition route via the HCOO or

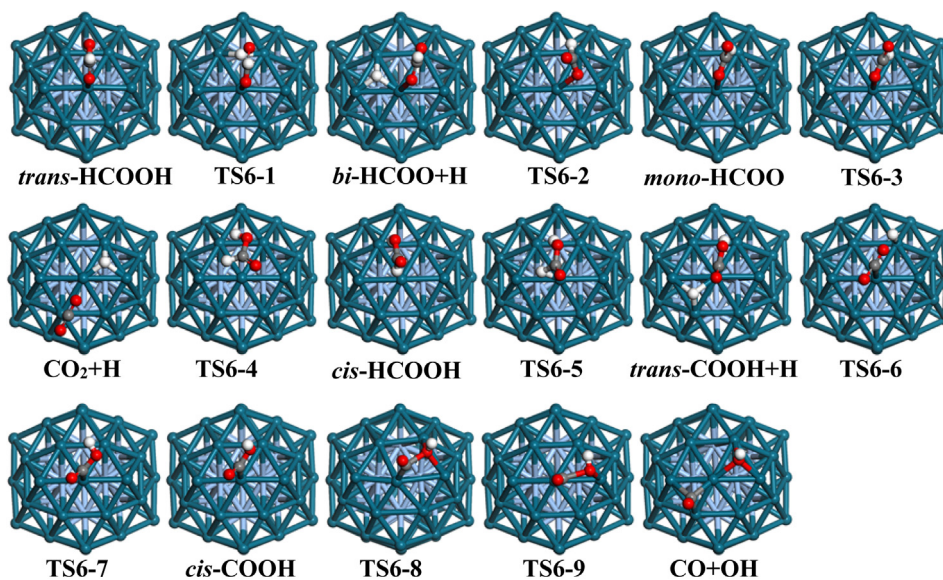
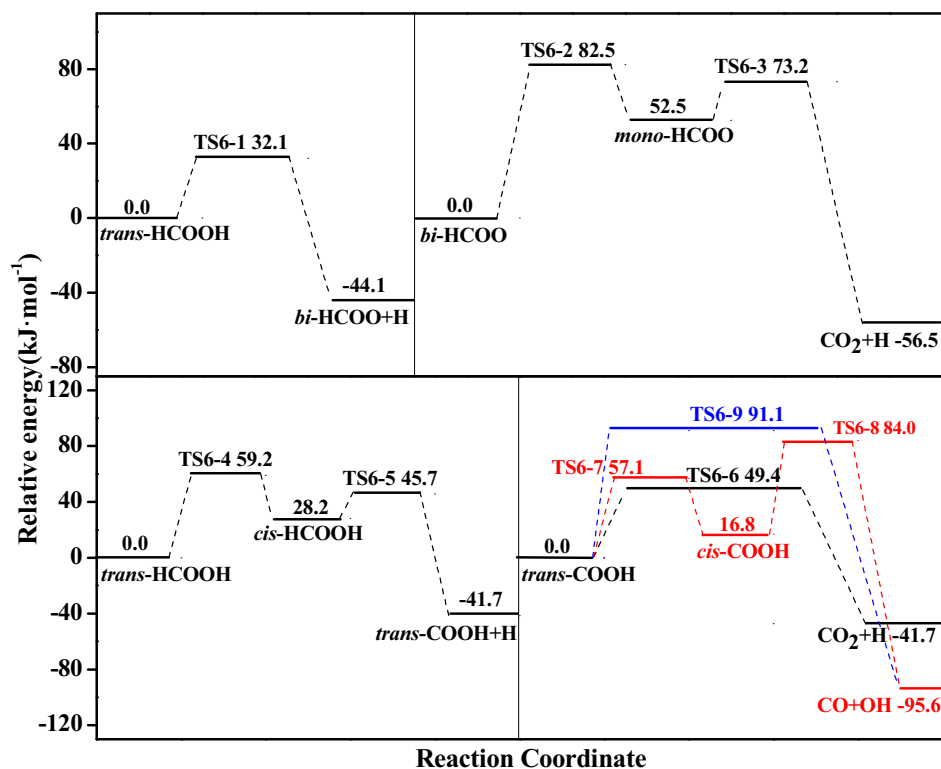


Fig. 7. Potential energy profile of HCOOH decomposition via the HCOO and COOH intermediates with the initial state, transition states and final states on Ag₁₃@Pd₄₂ at 298 K.

COOH intermediate, CO₂ prefers to be formed through the COOH intermediate; meanwhile, CO₂ can be also formed via the HCOO intermediate on different size of pure Pd and Ag-modified Pd nanoclusters.

Based on above results, HCOOH decomposition prefers to undergo COOH intermediate route to produce CO and CO₂, respectively; alternatively, CO₂ can be also formed via the HCOO intermediate route over different sizes of Pd and Ag-modified Pd nanoclusters, suggesting that the cluster size of the pure Pd and Ag-modified Pd nanoclusters has weak effect on the optimal route of HCOOH decomposition to form CO and CO₂. However, compared to the pure Pd nanoclusters, the composition in the Ag-modified Pd nanoclusters changes the optimal route of HCOOH decomposition to form CO.

3.4.2. The reason why COOH dissociation is more favorable CO₂ rather than CO

As mentioned above, the formation of CO and CO₂ in HCOOH decomposition undergoes the common *trans*-COOH intermediate; moreover, *trans*-COOH dissociation is more favorable for CO₂ formation via the O-H bond cleavage in kinetics rather than CO formation via the C-O bond cleavage. To better clarify the reason, the differential charge density of *trans*-COOH intermediate over the pure and Ag-modified Pd nanoclusters were analyzed. As shown in Fig. 8, the charge accumulation between H atom and catalyst surface makes the O-H bond cleavage more easily to generate CO₂ on the Pd_n (n = 13,38,55) and Ag_m@Pd_n (m + n = 13,38,55). In other words, there is an electron group of H atom toward the catalyst, which is beneficial to the O-H bond breakage to produce CO₂.

Moreover, the dissociated H species have stronger adsorption energy than the dissociated OH species via the C-O bond cleavage. In addition, starting from *trans*-COOH intermediate, previous studies also supported our calculated results, for example, the studies by Zhang *et al.* (Zhang *et al.*, 2012; Duan *et al.*, 2016) found that the O-H bond cleavage was much favored in kinetics than the C-O bond cleavage on the periodic Pd(111), Pt(111) and Pt_{ML}Au(111) surfaces, which was also similar to the studies by Scaranto and Mavrikakis on Pd(111) surface (Scaranto and Mavrikakis, 2016). He *et al.* (He *et al.*, 2016) investigated the catalytic activity of Cu₁@Pd₃(111) in HCOOH dissociation, indicating that *trans*-COOH is more favorable for CO₂ formation in kinetics than CO formation.

3.4.3. The effects of cluster size and composition on catalytic performance

To better understand the effect of cluster size and composition on catalytic performance of HCOOH decomposition, firstly, the activation barrier difference of the rate-controlled step between CO₂ and CO formation in the optimal formation path is used as a descriptor (Wang *et al.*, 2014; Yang *et al.*, 2020; Zhang *et al.*, 2019) to quantify the effect of cluster size and composition on the selectivity of HCOOH decomposition. More negative difference

signifies more favorable formation of CO₂ and the lower CO production. As shown in Fig. 9, the activation barrier differences between CO₂ and CO are -40.8, -36.9, -10.5 and -8.3 kJ·mol⁻¹ over the Pd₁₃, Pd₃₈, Pd₅₅ and Pd(111); those are -38.9, -40.7, -24.8 and -22.0 kJ·mol⁻¹ over the Ag₁@Pd₁₂, Ag₆@Pd₃₂, Ag₆@Pd₃₂ and Ag@Pd(111), respectively. Moreover, the activation barriers for the rate-controlled step of CO formation via the COOH intermediate and CO₂ formation via the HCOO intermediate showed that CO₂ formation is also energetically competitive or favorable than CO formation, namely, there are HCOO intermediate in HCOOH decomposition to form CO₂. Thus, DFT results show that CO₂ is the dominant product on the pure and Ag-modified Pd clusters; moreover, CO₂ selectivity decreases with the increasing of nanocluster size.

On the other hand, microkinetic modeling (Liu *et al.*, 2003; Cho *et al.*, 2017; Ling *et al.*, 2017; Choi and Liu, 2009) were further employed to investigate the activity and selectivity of HCOOH on different sizes of Pd and Ag-modified Pd catalysts, which can well consider the effects of reaction temperature, pressure ($P_{\text{HCOOH}} = 1$ atm, $T = 298$ K), and the terms of surface coverage for all intermediates in HCOOH decomposition under the realistic conditions. As listed in Table 1, microkinetic modeling results show that CO₂ selectivity in HCOOH decomposition on different sizes of Pd and

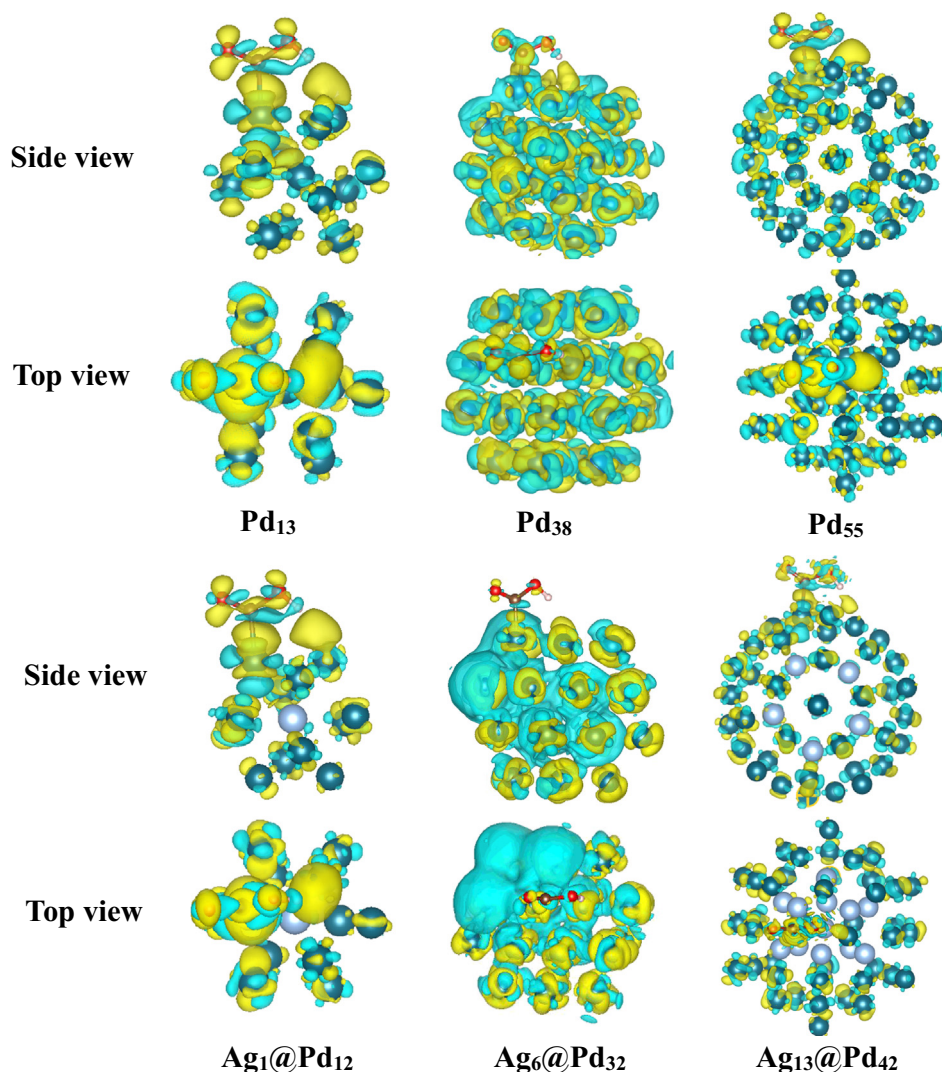


Fig. 8. The charge redistribution with the difference charge density for *trans*-COOH intermediate over the Pd₁₃, Pd₃₈, Pd₅₅, Ag₁@Pd₁₂, Ag₆@Pd₃₂, Ag₁₃@Pd₄₂ nanoclusters. The blue and yellow shaded regions represent the charge loss and charge gain, respectively.

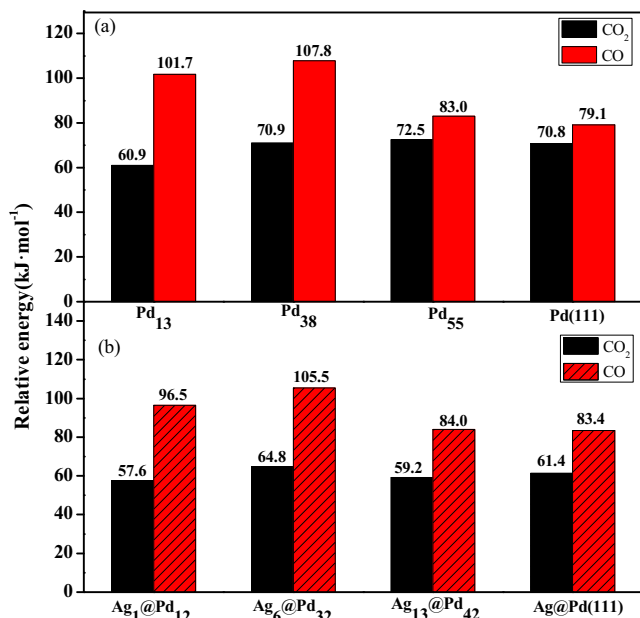


Fig. 9. The activation barrier of the rate-controlled step for the optimal path of HCOOH decomposition over the Pd₁₃, Pd₃₈, Pd₅₅, Ag₁@Pd₁₂, Ag₆@Pd₃₂, Ag₁₃@Pd₄₂ nanoclusters, Pd(111) and Ag@Pd(111) surfaces (Yang et al., 2020).

Ag-modified Pd nanoclusters can reach 99.90%; meanwhile, the high surface coverage of HCOO intermediate is involved in the route of HCOOH decomposition to form CO₂, namely, HCOO intermediate route mainly contributes to CO₂ formation under the realistic experiment conditions. Overall, DFT and microkinetic modeling results show that CO₂ is the dominant product on the pure and Ag-modified Pd clusters irrespective of the cluster size and composition.

As shown in Fig. 9(a), DFT results show that CO₂ formation has the activation barriers of 60.9, 70.9, 72.5 and 70.8 kJ·mol⁻¹ over the Pd₁₃, Pd₃₈, Pd₅₅ and Pd(111), respectively; moreover, as listed in Table 1, microkinetic modeling results show that the corresponding rates of CO₂ formation are 4.16×10^{-11} , 6.63×10^{-19} , 4.67×10^{-20} and 1.07×10^{-16} s⁻¹·site⁻¹; namely, the activity of CO₂ formation follows the order of Pd₁₃ ≫ Pd(111) > Pd₃₈ > Pd₅₅. As shown in Fig. 9(b), those of CO₂ are 57.6, 64.8, 59.2 and 61.4 kJ·mol⁻¹ over the Ag₁@Pd₁₂, Ag₆@Pd₃₂, Ag₁₃@Pd₄₂ and Ag@Pd(111), respectively; the corresponding rates of CO₂ formation are 5.57×10^{-11} , 1.26×10^{-15} , 8.52×10^{-14} and 1.99×10^{-17} s⁻¹·site⁻¹; namely, the activity of CO₂ formation follows the order of Ag₁@Pd₁₂ ≫ Ag₁₃@Pd₄₂ > Ag₆@Pd₃₂ > Ag@Pd(111). Thus, the pure and Ag-modified Pd nanocluster with the small size exhibit higher activity toward CO₂ formation in HCOOH

decomposition. Moreover, when the size of the pure and Ag-modified Pd nanocluster is the same, compare to the pure Pd, the composition in the Ag-modified Pd improves the activity of HCOOH decomposition to form CO₂.

The adsorption of HCOOH, HCOO and COOH intermediates involving in HCOOH decomposition are very key for the activation of these intermediates to form CO₂, as listed in Table S1, HCOOH, HCOO and COOH adsorption energies on the Pd_n(n = 13,38,55) and Ag_m@Pd_n(m + n = 13,38,55) nanoclusters generally decrease with the increasing of the cluster size, namely, the Pd₁₃ and Ag₁@Pd₁₂ nanoclusters is more favored for the adsorption of these intermediates due to the lower surface metal-coordination numbers in comparison with those on the Pd_n(n = 38,55) and Ag_m@Pd_n(m + n = 38,55) nanoclusters due to the higher metal-coordination numbers. Further, the projected density of states and *d*-band analysis were carried out to give out a physical explanation of this phenomenon, the *d*-band center (ϵ_d) of surface Pd atoms on the pure and Ag-modified Pd nanoclusters are analyzed, as shown in Fig. 10, among the Pd_n(n = 13,38,55), Ag_m@Pd_n(m + n = 13,38,55) nanoclusters, Pd(111) and Ag@Pd(111) surfaces, with the decreasing of the nanocluster size, the ϵ_d for Pd atoms is shifted upward, meanwhile, a upward shift of ϵ_d would lead to the weak interaction between the adsorbed species and metal nanoclusters (Li and Eric Croiset, 2012; Huo et al., 2009). This result well explains the higher adsorption energies of HCOOH, HCOO and COOH intermediates on the Pd₁₃ and Ag₁@Pd₁₂ nanoclusters than those on the Pd_n(n = 38,55) and Ag_m@Pd_n(m + n = 38,55) nanoclusters, thus, Pd₁₃ and Ag@Pd₁₂ are more favorable for the adsorption and activation of HCOOH, HCOO and COOH intermediates to form CO₂ in comparison with Pd_n(n = 38,55) and Ag_m@Pd_n(m + n = 38,55).

As shown in Figs. 2–7, HCOOH dehydrogenation to HCOO and COOH, as well as HCOO and COOH dehydrogenation to form CO₂ on the pure and Ag-modified Pd₁₃ nanoclusters is still energetically favored or competitive compared to other large sizes of the pure and Ag-modified Pd nanoclusters. Correspondingly, the ϵ_d of Pd₁₃ (-1.31 eV) and Ag₁@Pd₁₂ (-1.29 eV) are much close to the Fermi level corresponding to better activity toward HCOOH dehydrogenation to form CO₂ among these types of catalysts. Moreover, compared to Pd_n(n = 13,38,55), the ϵ_d of Ag_m@Pd_n(m + n = 13,38,55) with the same size is also close to the Fermi level, which present better catalytic activity, the promoter Ag changes the activity by changing the *d*-band center of Pd catalysts. In general, the closer the ϵ_d from the Fermi level is, the better the activity of CO₂ formation is, which provides physical origin of the difference for the activity of HCOOH decomposition to CO₂ on the Pd_n(n = 13,38,55) and Ag_m@Pd_n(m + n = 13,38,55) nanoclusters.

In summary, the small particles of the pure Pd and Ag-modified Pd nanoclusters exhibit better activity and selectivity toward HCOOH decomposition to produce CO₂. For the pure Pd nanocluster, our results are consistent with the experiments (Huang et al.,

Table 1

The formation rates (s⁻¹·site⁻¹) of CO₂ and CO over the Pd₁₃, Pd₃₈, Pd₅₅, Pd(111) (Yang et al., 2020); Ag₁@Pd₁₂, Ag₆@Pd₃₂, Ag₁₃@Pd₄₂ and Ag@Pd(111) surfaces (Yang et al., 2020) at 298 K, as well as the relative selectivity of CO₂ and CO.

| Catalysts | Formation rate | | Selectivity | |
|------------------------------------|------------------------|------------------------|-----------------|------|
| | CO ₂ | CO | CO ₂ | CO |
| Pd ₁₃ | 4.16×10^{-11} | 3.44×10^{-15} | 99.99 | 0.01 |
| Pd ₃₈ | 6.63×10^{-19} | 1.45×10^{-25} | 99.99 | 0.01 |
| Pd ₅₅ | 4.67×10^{-20} | 5.85×10^{-23} | 99.87 | 0.13 |
| Pd(111) | 1.07×10^{-16} | 4.94×10^{-20} | 99.99 | 0.01 |
| Ag ₁ @Pd ₁₂ | 5.57×10^{-11} | 1.02×10^{-15} | 99.99 | 0.01 |
| Ag ₆ @Pd ₃₂ | 1.26×10^{-15} | 7.59×10^{-22} | 99.99 | 0.01 |
| Ag ₁₃ @Pd ₄₂ | 8.52×10^{-14} | 1.51×10^{-20} | 99.99 | 0.01 |
| Ag@Pd(111) | 1.99×10^{-17} | 3.56×10^{-21} | 99.99 | 0.01 |

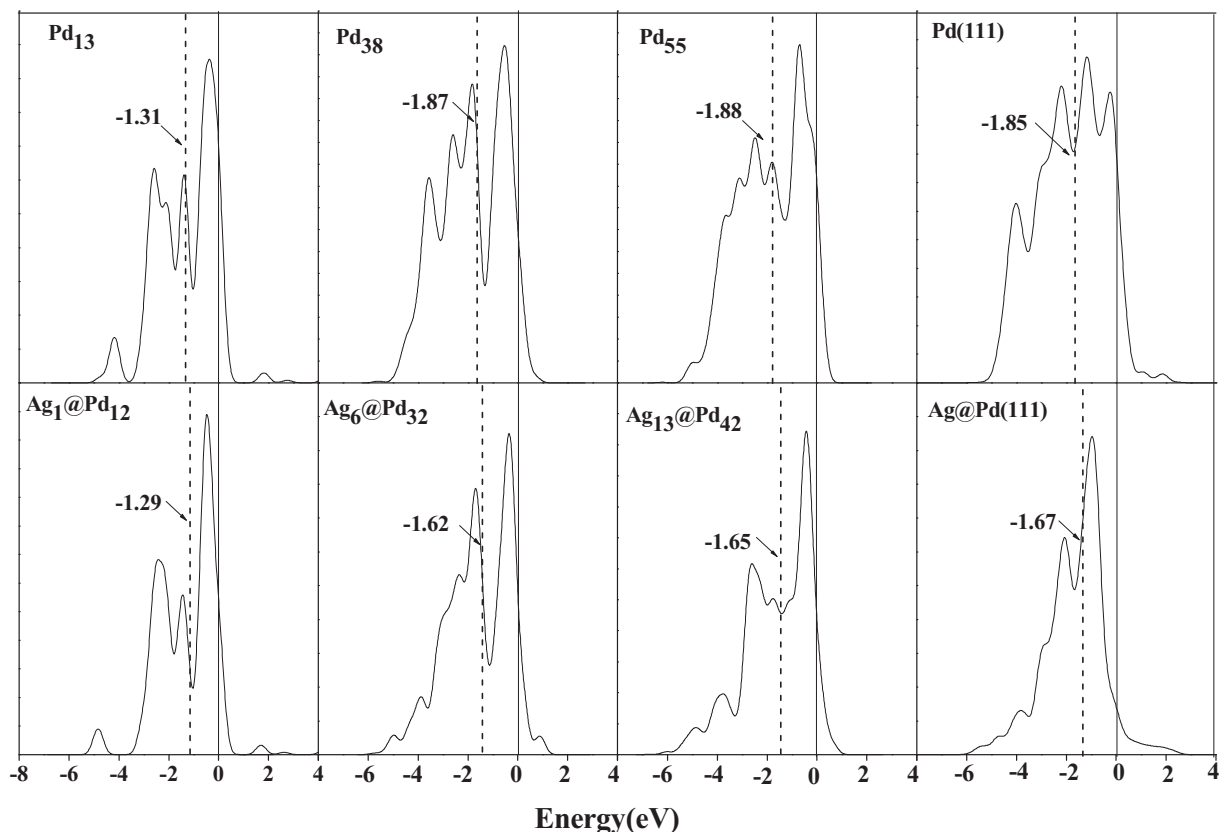


Fig. 10. Partial density of states for the surface Pd atoms of Pd₁₃, Pd₃₈, Pd₅₅, Ag₁@Pd₁₂, Ag₆@Pd₃₂, Ag₁₃@Pd₄₂ nanoclusters, Pd(111) and Ag@Pd(111) surfaces (Yang et al., 2020). The vertical dashed lines denote the location of the *d*-band center of surface Pd atom. The vertical solid lines represent the Fermi level.

2009; Kim and Kim, 2019; Zhou et al., 2006) that the smaller size of Pd nanoparticle exhibited higher activity and selectivity toward CO₂ formation in HCOOH decomposition. Meanwhile, compared to the pure Pd nanocluster, Ag_m@Pd_n nanocluster not only reduced the usage of precious metal Pd, but also exhibited better activity and selectivity toward HCOOH decomposition to form CO₂. Moreover, previous experimental results also supported our calculated results that Ag@Pd catalyst promoted the decomposition rate of HCOOH, for example, (Mori et al., 2013) believed that the activity of HCOOH decomposition to form CO₂ and H₂ strongly depended on the existence of the core Ag atom in the PdAg nanoparticles, which was obviously superior to the pure Pd and Ag catalysts. Jiang et al. (2012) concluded that Ag@Pd catalyst significantly improved the activity of HCOOH decomposition and enhanced the stability of Pd. Further, Tedsree et al. (2011) showed that Ag@Pd catalyst greatly increased the yield of CO₂ and H₂ in HCOOH decomposition compared to the pure Pd. Mandal and co-workers (Mandal et al., 2015) showed that the highest yield of H₂ in HCOOH decomposition was obtained over the AgPd catalyst with the Ag: Pd ratio of 1: 1.

4. Conclusions

In this study, the size and composition effects of the nanoclusters on the activity and selectivity of HCOOH decomposition on different sizes of pure and Ag-modified Pd nanoclusters was revealed using DFT calculations and microkinetic modeling. Pd_n (*n* = 13, 38, 55) and Ag_m@Pd_n (*m* + *n* = 13, 38, 55) nanoclusters were considered. The results show that HCOOH decomposition dominantly undergoes COOH intermediate to produce CO and CO₂ instead of that via HCOO intermediate, namely, HCOOH decomposition to form CO

and CO₂ undergoes common intermediate COOH irrespective of the cluster size and composition. Meanwhile, COOH dissociation is more favorable for CO₂ formation in kinetics than CO, which is attributed to that the charge accumulation between H atom and catalyst surface makes the O-H bond cleavage more easier on the Pd_n (*n* = 13, 38, 55) and Ag_m@Pd_n (*m* + *n* = 13, 38, 55). Further, small size of Pd₁₃ and Ag₁@Pd₁₂ nanoclusters present higher activity and selectivity toward CO₂ formation than large sizes of Pd_n (*n* = 38, 55) and Ag_m@Pd_n (*m* + *n* = 38, 55) nanoclusters; moreover, when the size of the pure and Ag-modified Pd nanocluster is same, compare to the pure Pd, Ag in the Ag-modified Pd improves the activity and selectivity of HCOOH decomposition to CO₂, and decrease the usage dose of noble metal Pd. The better catalytic performance for small size nanoclusters and Ag composition is attributed to that the *d*-band center is more close to the Fermi level. The results of this study not only clarify the effects of cluster size and composition on the activity and selectivity of HCOOH decomposition, but also provide a method to evaluate the catalytic performance of other Pd-based nanoclusters by adjusting the size of the nanocluster and changing the core metal type of the nanocluster.

CRediT authorship contribution statement

Min Yang: Writing - original draft, Writing - review & editing.
Baojun Wang: Formal analysis, Supervision, Data curation, Software.
Maohong Fan: Formal analysis, Writing - review & editing.
Riguang Zhang: Conceptualization, Writing - original draft, Writing - review & editing, Resources, Funding acquisition, Validation, Supervision, Project administration.

Declaration of Competing Interest

The authors declare that they have no known competing financial interests or personal relationships that could have appeared to influence the work reported in this paper.

Acknowledgment

This work is supported by the Key projects of National Natural Science Foundation of China (No. 21736007), the National Natural Science Foundation of China (No. 21776193) and the Top Young Innovative Talents of Shanxi. Also, authors appreciate the support of University of Wyoming.

Appendix A. Supplementary data

Supplementary data to this article can be found online at <https://doi.org/10.1016/j.ces.2020.116016>.

References

- Fellay, C., Dyson, P.J., Launicy, G.A., 2008. Viable hydrogen storage system based on selective formic acid decomposition with a ruthenium catalyst. *Angew. Chem. Int. Ed.* 47, 3966–3968.
- Zhang, S., Shao, Y.Y., Yin, G.P., Lin, Y.H., 2010. Electrostatic self-assembly of a Pt-around-Au nanocomposite with high activity towards formic acid oxidation. *Angew. Chem. Int. Ed.* 49, 2211–2214.
- Ha, S., Larsen, R., Masel, R.I., 2005. Performance characterization of Pd/C nanocatalyst for direct formic acid fuel cells. *J. Power Sources* 144, 28–34.
- Uhm, S., Lee, H.J., Kwon, Y., Lee, J., 2008. A stable and cost-effective anode catalyst structure for formic acid fuel cells. *Angew. Chem. Int. Ed.* 120, 10317–10320.
- Mori, K., Dojo, M., Yamashita, H., 2013. Pd and Pd-Ag nanoparticles within a macroreticular basic resin: an efficient catalyst for hydrogen production from formic acid decomposition. *ACS Catal.* 3, 1114–1119.
- Yang, Y., Xu, H.X., Cao, D.P., Zeng, X.C., Cheng, D.J., 2019. Hydrogen production via efficient formic acid decomposition: engineering the surface structure of Pd-based alloy catalysts by design. *ACS Catal.* 9, 781–790.
- Hu, S.Z., Che, F.L., Khorasani, B., Jeon, M., Yoon, C.W., McEwen, J.S., Scudier, L., Ha, S., 2019. Improving the electrochemical oxidation of formic acid by tuning the electronic properties of Pd-based bimetallic nanoparticles. *Appl. Catal. B: Environ.* 254, 685–692.
- Choi, B.S., Song, J., Song, M.J., Goo, B.S., Lee, Y.W., Kim, Y., Yang, H., Han, S.W., 2019. Core-shell engineering of Pd-Ag bimetallic catalysts for efficient hydrogen production from formic acid decomposition. *ACS Catal.* 9, 819–826.
- Rice, C., Ha, S., Masel, R.I., Waszczuk, P., Wieckowski, A., Barnard, T., 2002. Direct formic acid fuel cells. *J. Power Sources* 111, 83–89.
- Wang, Y.Y., Qi, Y.Y., Zhang, D.J., Liu, C.B., 2014. New insight into the decomposition mechanism of formic acid on Pd(111): competing formation of CO₂ and CO. *J. Phys. Chem. C* 118, 2067–2076.
- Brandt, K., Steinhilber, M., Wandelt, K., 2008. Catalytic and electro catalytic oxidation of formic acid on the pure and Cu-modified Pd(111)-surface. *J. Electroanal. Chem.* 616, 27–37.
- Wang, J.Y., Zhang, H.X., Jiang, K., Cai, W.B., 2011. From HCOOH to CO at Pd electrodes: a surface-enhanced infrared spectroscopy study. *J. Am. Chem. Soc.* 133, 14876–14879.
- El-Nagar, G.A., Darweesh, A.F., Sadiq, I., 2016. A novel nano-palladium complex anode for formic acid electro-oxidation. *Electrochim. Acta* 215, 334–338.
- Yu, X.W., Pickup, P.G., 2009. Mechanistic study of the deactivation of carbon supported Pd during formic acid oxidation. *Electrochem. Commun.* 11, 2012–2014.
- Gao, Y.W., Wang, G., Wu, B., Deng, C., Gao, Y., 2011. Highly active carbon-supported PdNi catalyst for formic acid electrooxidation. *J. Appl. Electrochem.* 41, 1–6.
- Shen, L.P., Li, H.Z., Lu, L., Luo, Y.F., Tang, Y.W., Chen, Y., Lu, T.H., 2013. Improvement and mechanism of electrocatalytic performance of Pd-Ni/C anodic catalyst in direct formic acid fuel cell. *Electrochim. Acta* 89, 497–502.
- Yu, W.Y., Mullen, G.M., Flaherty, D.W., Mullins, C.B., 2014. Selective hydrogen production from formic acid decomposition on Pd-Au bimetallic surfaces. *J. Am. Chem. Soc.* 136, 11070–11078.
- Gu, X.J., Lu, Z.H., Jiang, H.L., Akita, T., Xu, Q., 2011. Synergistic catalysis of metal-organic framework-immobilized Au-Pd nanoparticles in dehydrogenation of formic acid for chemical hydrogen storage. *J. Am. Chem. Soc.* 133, 11822–11825.
- Lu, Y.Z., Chen, W., 2012. PdAg alloy nanowires: facile one-step synthesis and high electrocatalytic activity for formic acid oxidation. *ACS Catal.* 2, 84–90.
- Tedsree, K., Li, T., Jones, S., Chan, C.W.A., Yu, K.M.K., Bagot, P.A.J., Marquis, E.A., Smith, G.D.W., Tsang, S.C.E., 2011. Hydrogen production from formic acid decomposition at room temperature using a Ag-Pd core-shell nanocatalyst. *Nat. Nanotechnol.* 6, 302–307.
- Wang, R.X., Fan, Y.J., Liang, Z.R., Zhang, J.M., Zhou, Z.Y., Sun, S.G., 2016. PdSn nanocatalysts supported on carbon nanotubes synthesized in deep eutectic solvents with high activity for formic acid electrooxidation. *RSC Adv.* 6, 60400–60406.
- Sun, D.D., Si, L., Fu, G.T., Liu, C., Sun, D.M., Chen, Y., Tang, Y.W., Lu, T.H., 2015. Nanobranched porous palladium-tin intermetallics: one-step synthesis and their superior electrocatalysis towards formic acid oxidation. *J. Power Sources* 280, 141–146.
- Dai, L., Zou, S.Z., 2011. Enhanced formic acid oxidation on Cu-Pd nanoparticles. *J. Power Sources* 196, 9369–9372.
- Wu, D.F., Xu, H.X., Cao, D.P., Fisher, A., Gao, Y., Cheng, D.J., 2016. PdCu alloy nanoparticle-decorated copper nanotubes as enhanced electrocatalysts: DFT prediction validated by experiment. *Nanotechnology* 27, 495403–495413.
- Huang, Y., Zhou, X., Yin, M., Liu, C.P., Xing, W., 2010. Novel PdAu@Au/C core-shell catalyst: superior activity and selectivity in formic acid decomposition for hydrogen generation. *Chem. Mater.* 22, 5122–5128.
- Feng, L.G., Chang, J.F., Jiang, K., Xue, H.G., Liu, C.P., Cai, W.B., Xing, W., Zhang, J.J., 2016. Nanostructured palladium catalyst poisoning depressed by cobalt phosphide in the electro-oxidation of formic acid for fuel cells. *Nano Energy* 30, 355–361.
- Maroun, F., Ozanam, F., Magnussen, O.M., Behm, R.J., 2001. The role of atomic ensembles in the reactivity of bimetallic electrocatalysts. *Science* 293, 1811–1814.
- Fan, Y., Zhang, Y., Li, H.M., Shen, W.M., Wang, J.L., Wei, M.M., 2016. Three-dimensional highly branched Pd₃Cu alloy multipods as enhanced electrocatalysts for formic acid oxidation. *RSC Adv.* 6, 43980–43984.
- Liu, D., Gao, Z.Y., Wang, X.C., Zeng, J., Li, Y.M., 2017. DFT study of hydrogen production from formic acid decomposition on Pd-Au alloy nanoclusters. *Appl. Surf. Sci.* 426, 194–205.
- Li, S.J., Cheng, D.J., Qiu, X.G., Cao, D.P., 2014. Synthesis of Cu@Pd core-shell nanowires with enhanced activity and stability for formic acid oxidation. *Electrochim. Acta* 143, 44–48.
- Zhou, X.C., Huang, Y.J., Xing, W., Liu, C.P., Liao, J.H., Lu, T.H., 2008. High-quality hydrogen from the catalyzed decomposition of formic acid by Pd-Au/C and Pd-Ag/C. *Chem. Commun.* 30, 3540–3542.
- Huang, L., Yang, J., Wu, M., Shi, Z.Q., Lin, Z., Kang, X.W., Chen, S.W., 2018. PdAg@Pd core-shell nanotubes: superior catalytic performance towards electrochemical oxidation of formic acid and methanol. *J. Power Sources* 398, 201–208.
- Yang, M., Wang, B.J., Li, Z.Q., Ling, L.X., Zhang, R.G., 2020. HCOOH dissociation over the core-shell M@Pd bimetallic catalysts: probe into the effect of the core metal type on the catalytic performance. *Appl. Surf. Sci.* 506, 144938–144950.
- Zhao, B., Zhang, R.G., Huang, Z.X., Wang, B.J., 2017. Effect of the size of Cu clusters on selectivity and activity of acetylene selective hydrogenation. *Appl. Catal. A: Gen.* 546, 111–121.
- Huang, Y.J., Liao, J.H., Liu, C.P., Lu, T.H., Xing, W., 2009. The size-controlled synthesis of Pd/C catalysts by different solvents for formic acid electrooxidation. *Nanotechnology* 20, 105604–105609.
- Li, S.J., Zhou, X., Tian, W.Q., 2012. Theoretical investigations on decomposition of HCOOH catalyzed by Pd₇ cluster. *J. Phys. Chem. A* 116, 11745–11752.
- Kresse, G., Furthmüller, J., 1996a. Efficiency of ab-initio total energy calculations for metals and semiconductors using a plane-wave basis set. *Comput. Mater. Sci.* 6, 15–50.
- Kresse, G., Furthmüller, J., 1996b. Efficient iterative schemes for ab-initio total-energy calculations using a plane-wave basis set. *Phys. Rev. B* 54, 11169–11186.
- Blöchl, P.E., 1994. Projector augmented-wave method. *Phys. Rev. B: Condens. Matter.* 50, 17953–17979.
- Perdew, J.P., Wang, Y., 1992. Accurate and simple analytic representation of the electron-gas correlation energy. *Phys. Rev. B* 45, 13244–13249.
- Perdew, J.P., Burke, K., Ernzerhof, M., 1996. Generalized gradient approximation made simple. *Phys. Rev. Lett.* 77, 3865–3868.
- Sheppard, D., Xiao, P.H., Chemelewski, W., Johnsonand, D.D., Henkelman, G., 2012. A generalized solid-state nudged elastic band method. *J. Phys. Chem.* 136, 074103–074108.
- Sheppard, D., Terrell, R., Henkelman, G., 2008. Optimization methods for finding minimum energy paths. *J. Chem. Phys.* 128, 385–404.
- Henkelman, G., Jónsson, H., 1999. A dimer method for finding saddle points on high dimensional potential surfaces using only first derivatives. *J. Phys. Chem.* 111, 7010–7022.
- Olsen, R.A., Kroes, G.J., Henkelman, G., Arnaldsson, A., 2004. Comparison of methods for finding saddle points without knowledge of the final states. *J. Phys. Chem.* 121, 9776–9792.
- Soler, J.M., Beltrán, M.R., Michaelian, K., Garzón, I.L., Ordejón, P., Sánchez-Portal, D., Artacho, E., 2000. Metallic bonding and cluster structure. *Phys. Rev. B* 61, 5771–5780.
- Nayak, S.K., Jena, P., Stepanyuk, V.S., Hergert, W., Wildberger, K., 1997. Magic numbers in supported metal clusters. *Phys. Rev. B* 56, 6952–6957.
- Karabacak, M., Özçelik, S., Güvenc, Z.B., 2003. Structures and energetics of Pd₂₁-Pd₅₅ clusters. *Surf. Sci.* 532, 306–311.
- Rapps, T., Ahlrichs, R., Waldt, E., Kappes, M.M., Schooss, D., 2013. On the structures of 55-atom transition-metal clusters and their relationship to the crystalline bulk. *Angew. Chem. Int. Ed.* 52, 6102–6105.
- Zhu, J., Cheng, P., Wang, N., Huang, S.P., 2015. Insight into the structural and electronic properties of Pd₅₅-nNi_n (n = 0–55) clusters: a density functional theory study. *Comput. Theor. Chem.* 1071, 9–17.
- Kumar, V., Kawazoe, Y., 2003. Magnetism in clusters of non-magnetic elements: Pd, Rh, and Ru. *Eur. Phys. J. D* 24, 81–84.

- Zhao, J., Chen, X., Sun, Q., Wang, G., 1995. Critical size for magnetic-non-magnetic transition in transition metal clusters. *Europhys. Lett.* 32, 113–117.
- Zhang, R.G., Liu, H.Y., Wang, B.J., Ling, L.X., 2012. Insights into the preference of CO₂ formation from HCOOH decomposition on Pd surface: a theoretical study. *J. Phys. Chem. C* 116, 22266–22280.
- Singh, S., Li, S., Carrasquillo-Flores, R., Alba-Rubio, A.C., Dumesic, J.A., Mavrikakis, M., 2014. Formic acid decomposition on Au catalysts: DFT, microkinetic modeling, and reaction kinetics experiments. *AIChE J.* 60, 1303–1319.
- Qi, Y.Y., Gao, J., Zhang, D.J., Liu, C.B., 2015. Comparative theoretical study of formic acid decomposition on PtAg(111) and Pt(111) surfaces. *RSC Adv.* 5, 21170–21177.
- Zhang, R.G., Yang, M., Peng, M., Ling, L.X., Wang, B.J., 2019. Understanding the role of Pd: Cu ratio, surface, and electronic structures in Pd-Cu alloy material applied in direct formic acid fuel cell. *Appl. Surf. Sci.* 465, 730–790.
- Samjeske, G., Osawa, M., 2005. Current oscillations during formic acid oxidation on a Pt electrode: insight into the mechanism by time-resolved IR spectroscopy. *Angew. Chem. Int. Ed.* 44, 5694–5698.
- Gao, W., Keith, J.A., Anton, J., Jacob, T., 2012. Theoretical elucidation of the competitive electro-oxidation mechanisms of formic acid on Pt(111). *J. Am. Chem. Soc.* 132, 18377–18385.
- Herrero, E., Feliu, J.M., 2018. Understanding formic acid oxidation mechanism on platinum single crystal electrodes. *Curr. Opin. Electrochem.* 9, 145–160.
- Vela, M.E., Lezna, R.O., Detacconi, N.R., Arvia, A.J., Beden, B., Hahn, F., Lamy, C., 1992. EMIRS studies of formic acid electrooxidation on Pd, Au and Pd+Au alloys: Part 1. Investigation of the adsorbates derived from HCOOH and NACOOH chemisorption at Pd in acid and alkaline solutions. *J. Electroanal. Chem.* 323, 289–302.
- Chen, Y.X., Heinen, M., Jusys, Z., Behrn, R.J., 2006. Bridge-bonded formate: active intermediate or spectator species in formic acid oxidation on a Pt film electrode?. *Langmuir* 22, 10399–10408.
- Duan, T., Zhang, R.G., Ling, L.X., Wang, B.J., 2016. Insights into the effect of Pt atomic ensemble on HCOOH oxidation over Pt-decorated Au bimetallic catalyst to maximize Pt utilization. *J. Phys. Chem. C* 120, 2234–2246.
- Scaranto, J., Mavrikakis, M., 2016. Density functional theory studies of HCOOH decomposition on Pd(111). *Surf. Sci.* 650, 111–120.
- He, F., Li, K., Xie, G.Y., Wang, Y., Jiao, M.G., Tang, H., Wu, Z.J., 2016. Understanding the enhanced catalytic activity of Cu₁@Pd₃(111) in formic acid dissociation, a theoretical perspective. *J. Power Sources* 316, 8–16.
- Liu, P., Logadottir, A., Nørskov, J.K., 2003. Modeling the electro-oxidation of CO and H₂/CO on Pt, Ru, PtRu and Pt₃Sn. *Electrochim. Acta* 48, 3731–3742.
- Cho, J., Lee, S., Yoon, S.P., Han, J., Nam, S.W., Lee, K.Y., Ham, H.C., 2017. Role of heteronuclear interactions in selective H₂ formation from HCOOH decomposition on bimetallic Pd/M (M=late transition FCC metal) catalysts. *ACS Catal.* 7, 2553–2562.
- Ling, L.X., Zhao, Z.B., Feng, X., Wang, Q., Wang, B.J., Zhang, R.G., Li, D.B., 2017. Insight into the reduction of NO by H₂ on the stepped Pd(211) surface. *J. Phys. Chem. C* 121, 16399–16414.
- Choi, Y.M., Liu, P., 2009. Mechanism of ethanol synthesis from syngas on Rh(111). *J. Am. Chem. Soc.* 131, 13054–13061.
- Li, J.D., Eric Croiset, Ricardez-Sandoval, L., 2012. Methane dissociation on Ni(100), Ni(111), and Ni(553): A comparative density functional theory study. *J. Mol. Catal. A: Chem.* 365, 103–114.
- Huo, C.F., Li, Y.W., Wang, J.G., Jiao, H.J., 2009. Insight into CH₄ formation in iron-catalyzed Fischer-Tropsch synthesis. *J. Am. Chem. Soc.* 2009, 14713–14721.
- Kim, Y., Kim, D.H., 2019. Understanding the effect of Pd size on formic dehydrogenation via size-controlled Pd/C catalysts prepared by NaBH₄ treatment. *Appl. Catal. B: Environ.* 224, 684–693.
- Zhou, W.P., Lewera, A., Larsen, R., Masel, R.I., Bagus, P.S., Wieckowski, A., 2006. Size effects in electronic and catalytic properties of unsupported palladium nanoparticles in electrooxidation of formic acid. *J. Phys. Chem. B* 110, 13393–13398.
- Jiang, Y.Y., Lu, Y.Z., Han, D.X., Zhang, Q.X., Niu, L., 2012. Hollow Ag@Pd core-shell nanotubes as highly active catalysts for the electro-oxidation of formic acid. *Nanotechnology* 23, 105609–105619.
- Mandal, K., Bhattacharjee, D., Dasgupta, S., 2015. Synthesis of nanoporous PdAg nanoalloy for hydrogenation generation from formic acid at room temperature. *Int. J. Hydrogen Energy* 40, 4786–4793.